Supporting Information

Critical state-induced emergence of superior magnetic performances in an iron-based amorphous soft magnetic composite

Liliang Shao[1,2,7], Rongsheng Bai[1,3,7], Yanxue Wu[4], Jing Zhou[1], Xing Tong[1], Hailong Peng[4], Tao Liang[5], Zongzhen Li[6], Qiaoshi Zeng[5], Bo Zhang[1], Haibo Ke[1,*], Weihua Wang[1,2,3,*]

[1] Songshan Lake Materials Laboratory, Dongguan 523808, China

[2] Institute of Physics, Chinese Academy of Sciences, Beijing 100190, China

[3] School of Energy, Power and Mechanical Engineering, North China Electric Power University, Beijing 100096, China

[4] School of Materials Science and Engineering, Central South University, Changsha 410083, China

[5] Center for High Pressure Science and Technology Advanced Research, Shanghai 201203, China

[6] Jiangsu JITRI Advanced Energy Materials Research Institute Co., Ltd., Changzhou 213000, China

*Corresponding author: Haibo Ke (E-mail: kehaibo@sslab.org.cn) and Weihua Wang (E-mail: whw@iphy.ac.cn)

[7]These authors contributed equally to this work.

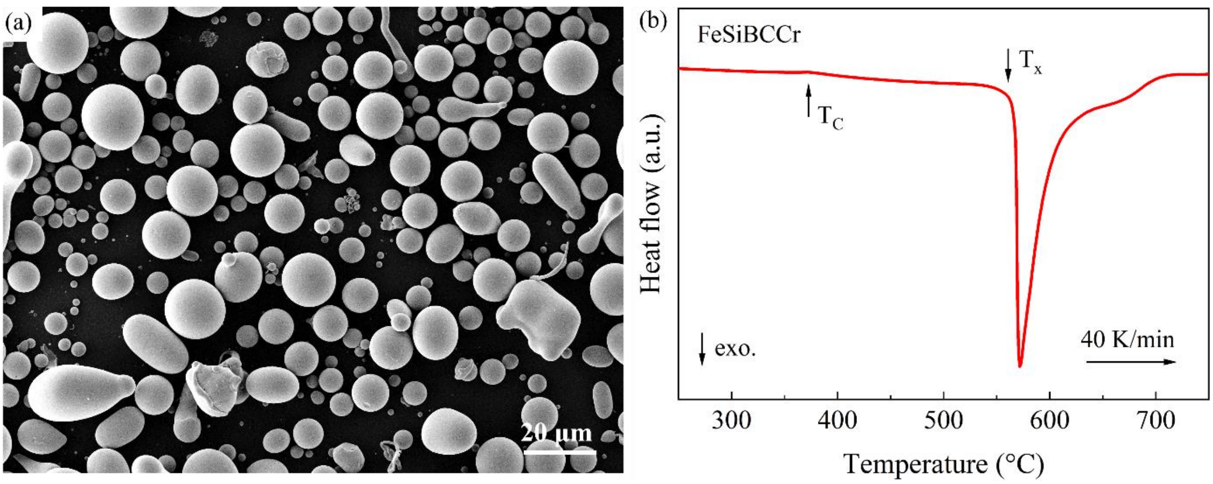

Figure S1. Morphology and thermal analysis of the FeSiBCCr amorphous powder. (a) SEM image and (b) DSC curve of the atomized FeSiBCCr powder under the heating rate of 40 K/min.

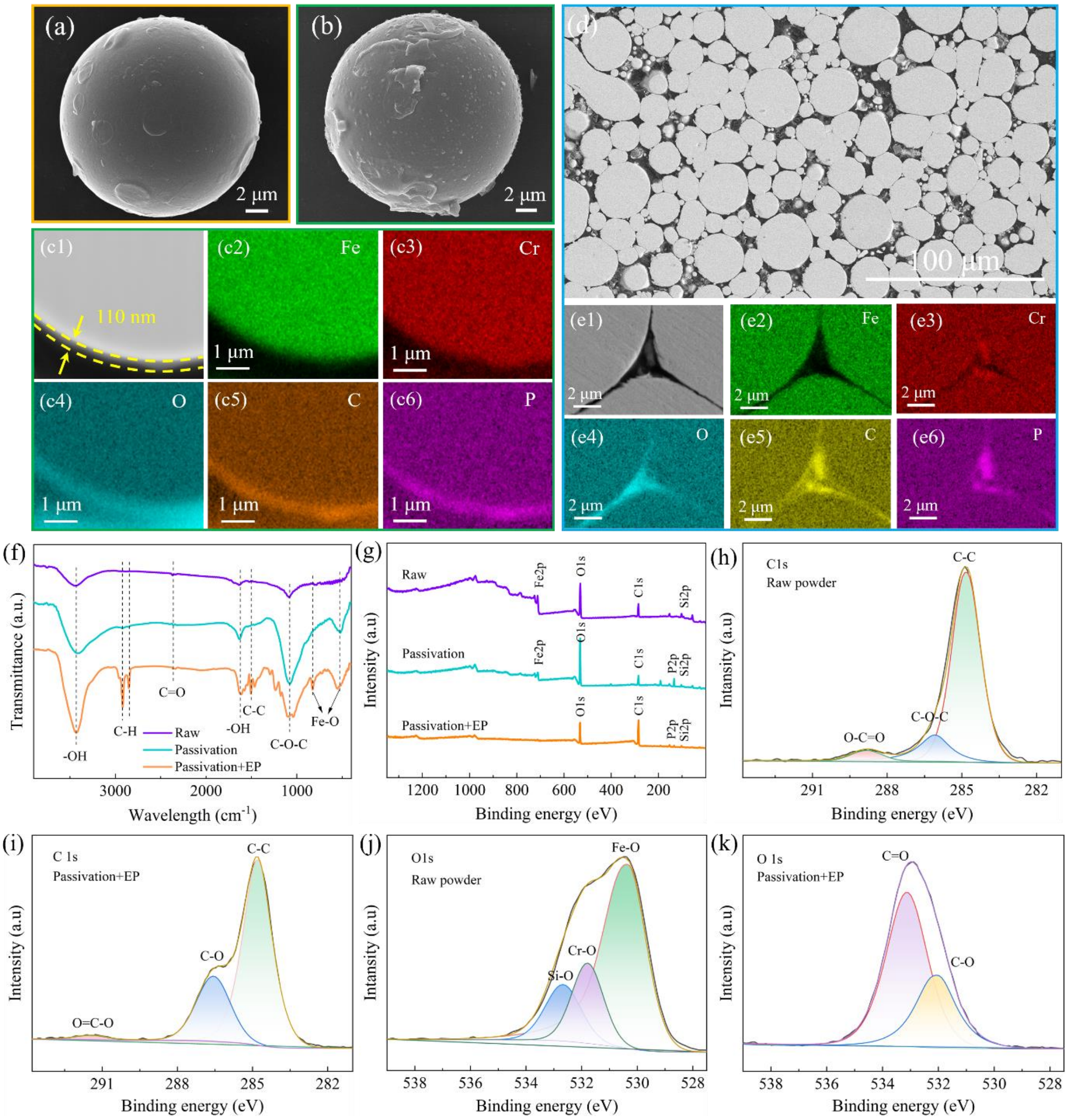

Figure S2. Characterizations of the coating layer of the ASMC. SEM images of the (a) passivated and (b) EP coating powders; (c1) Cross-sectional morphology of the coated powder; (c2-c6) Magnification of the polished cross-section and corresponding EDS images of the ASMC; (d) Cross-section of the ASMC and (e1-e6) corresponding EDS mappings. (f) FTIR spectra of the raw, passivated and coated powders; (g) XPS spectra of the raw, passivated and coated powders; Zoomed-in C1s peak of the (h) raw and (i) insulated powders; Zoomed-in O1s peak of the (j) raw and (k) insulated powders.

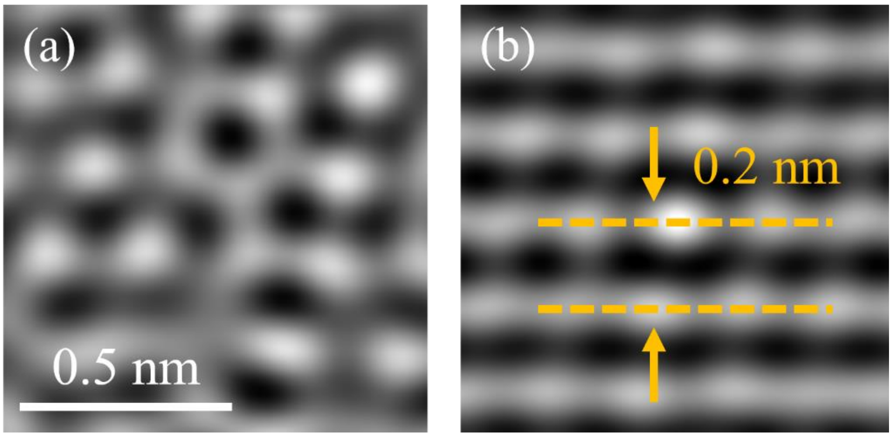

Figure S3. (a) HRTEM image of the local crystal-like order dispersed in the FeSiBCCr amorphous matrix. (b) Corresponding image after auto-correlation function transform. The distance between two fringes is ~0.2 nm, consisting with the interplanar spacing of (1 1 0) plane in *α*-Fe phase.

Figure S4(a) shows the HRTEM image of the original FeSiBCCr amorphous powder, exhibiting a typical maze-like pattern without detectable crystalline structure. Figure S4(b) presents the 2D-ACF segments of the region in figure S4(a). The areal fraction of critical structures marked by red and green squares are 11.3%.

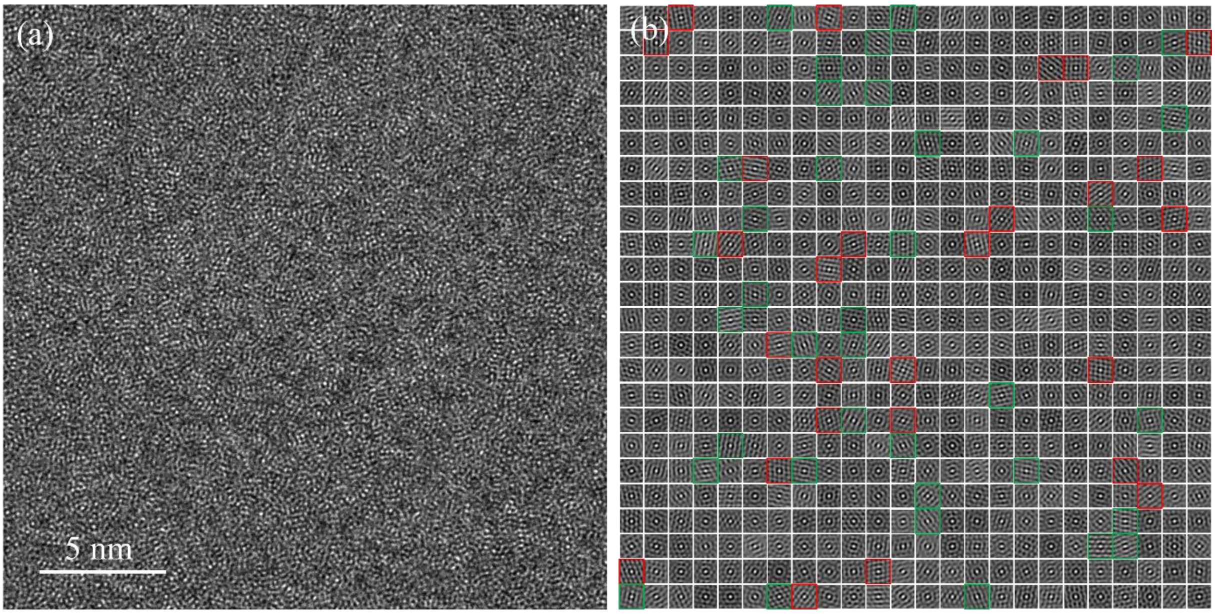

Figure S4. (a) HRTEM image and (b) corresponding 2D-ACF mappings of the as-atomized FeSiBCCr amorphous powder, each cell with a size of 1.01×1.01 nm^2.

Figure S5 displays the temperature dependence of M_s and μ_e of the FeSiBCCr SMCs. It can be seen that both M_s and μ_e obtain maximum values at the 475-RFA, corresponding to the critical-state amorphous powder.

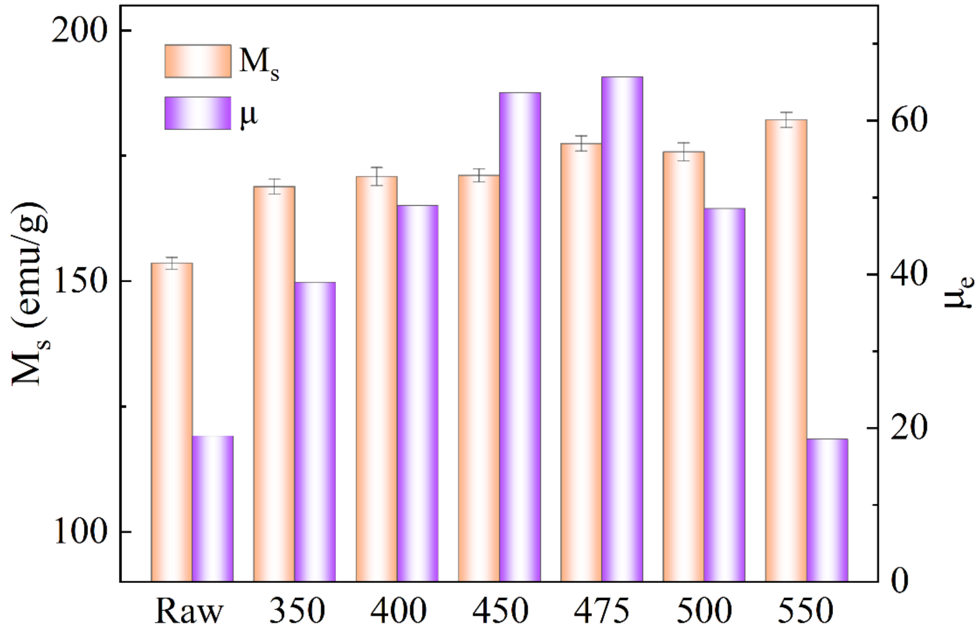

Figure S5. Variations of M_s and μ_e of the FeSiBCCr SMCs annealed under different conditions

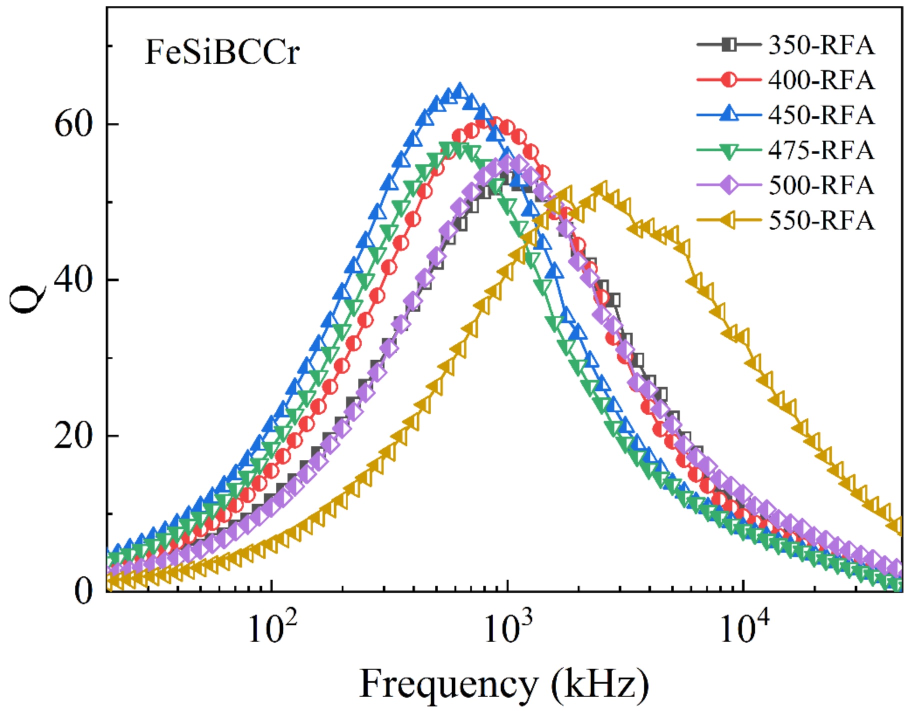

Figure S6. Frequency dependence of quality factor (Q) for the annealed ASMCs

To clarify the effect of annealing treatment on P_{cv}, loss separation was carried out. In general, the total magnetic core loss P_{cv} of ASMCs can be divided into three parts: hysteresis loss (P_h), eddy current loss (P_e) and residual loss (P_r) as depicted by Eq. (1) [1].

$$P_{cv} = P_h + P_e + P_{ex} = K_h B_m^n f + K_e B_m^2 f^2 + K_r B_m^{1.5} f^{1.5} \quad (1)$$

Where, K_h, K_e and K_r denote hysteresis, eddy current and excess loss coefficients, and B_m, f are magnetic flux density and frequency. Among them, P_r originates from relaxation and resonance losses and is usually negligible at low and ultra-high frequencies [2,3]. As displayed in figure S7(a), P_{cv}/f versus f can be well fitted by linear function, indicating the P_{cv} of the studied FeSiBCCr ASMCs is mainly composed of P_h and P_e. Therefore, the P_{cv} in this study is expressed by Eq. (2). The loss separation was performed according to the equation.

$$P_{cv} = P_h + P_e = K_h B_m^n f + K_e B_m^2 f^2 \quad (2)$$

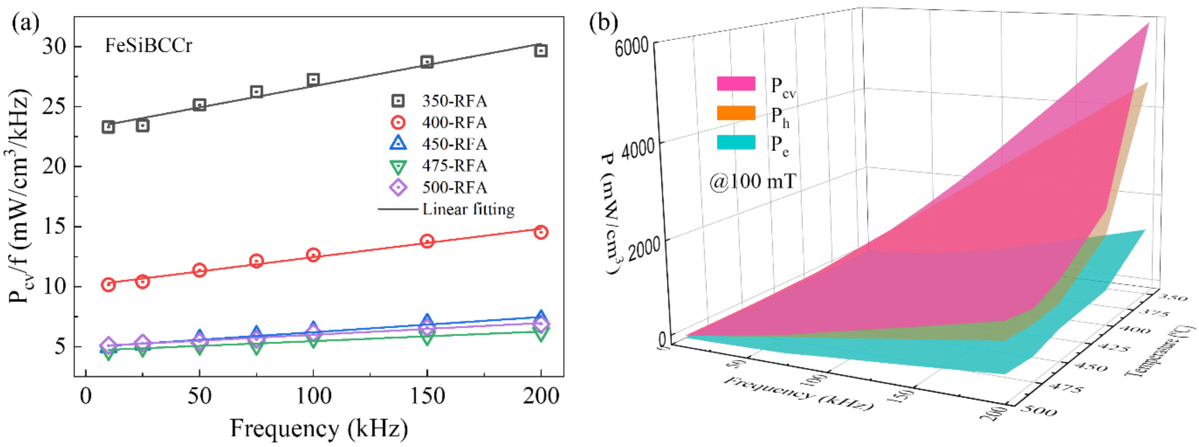

Figure S7. (a) The relationship between frequency and P_{cv}/f and (b) corresponding loss separation of the ASMCs annealed at different temperatures

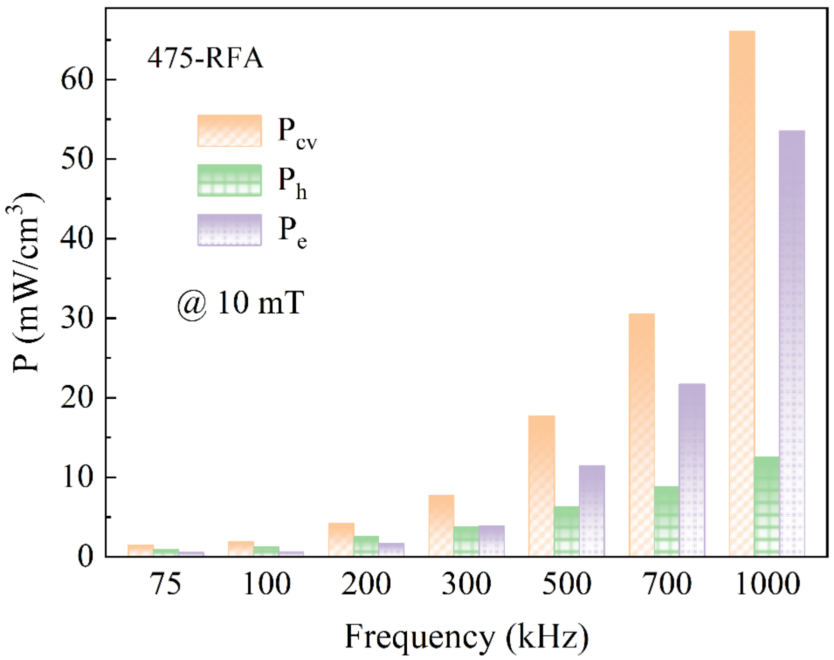

Figure S8. Variation of P_{cv}, P_h and P_e from 75 kHz to 1 MHz for the 475-RFA ASMCs.

Figure S9 shows the MFM image of the FeSiBCCr SMC annealed at 500-RFA. Although some large-scale crystals precipitate in amorphous matrix, the magnetic domain exhibits typical strip feature, and thus the 500-RFA SMC possess better magnetic softness compared with the original SMC, i.e., higher μ_e and lower P_{cv}.

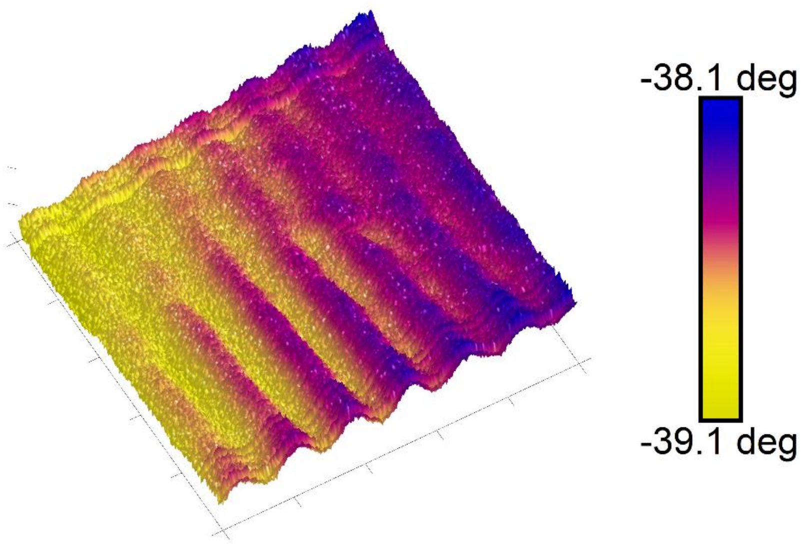

Figure S9. 3D-MFM image of the 500-RFA SMC.

References

[1] Taghvaei A H, Shokrollahi H, Janghorban K and Abiri H 2009 Eddy current and total power loss separation in the iron-phosphate-polyepoxy soft magnetic composites *Mater. Design* **30** 3989-3995.

[2] Shokrollahi H and Janghorban K 2007 Soft magnetic composite materials (SMCs) *J. Mater. Process. Tech.* **189** 1-12.

[3] Zhang Y Q et al 2020 Poly-para-xylylene enhanced Fe-based amorphous powder cores with improved soft magnetic properties via chemical vapor deposition *Mater. Design* **191** 108650.